

Zooming-in on Instantons at HERA

A. Ringwald and F. Schrempp

Deutsches Elektronen-Synchrotron DESY, Hamburg, Germany

Abstract

In view of the intriguing, preliminary search results for instanton-induced events at HERA from the H1 collaboration, some important remaining theoretical issues are discussed. Notably, the question is addressed, to which extent the H1 analysis may be directly compared to our original predictions from instanton-perturbation theory, since certain fiducial cuts are lacking in the H1 data. Various theoretical uncertainties are evaluated and their impact on the observed excess is discussed. An improved understanding of the experimental findings along with an encouraging over-all agreement with our original predictions seems to emerge.

1. Instantons represent a basic non-perturbative aspect of QCD, theoretically discovered and first studied by Belavin *et al.* [1] and 't Hooft [2], about 25 years ago. As topologically non-trivial fluctuations of the gauge fields with a typical size of $0.3 \div 0.5$ fm [3, 4, 5], instantons play an important rôle in the transition region between a partonic and a hadronic description of strong interactions [6]. Yet, despite substantial theoretical evidence for the importance of instantons in chiral symmetry breaking and hadron spectroscopy, their direct experimental verification is lacking until now.

It turns out, however, that a characteristic *short distance* manifestation of instantons can be exploited [7] for an experimental search: Instantons induce certain (hard) processes that are forbidden in usual perturbative QCD. These involve all (light) quark flavours democratically along with a violation of chirality, in accord with the general chiral anomaly relation [2].

Deep-inelastic scattering (DIS) at HERA offers a unique opportunity [7] to discover these hard processes induced by QCD-instantons. It is of particular importance that a theoretical prediction of both the corresponding rate [8, 9, 10] and the characteristic event signature [7, 11, 12] is possible in this hard scattering regime¹. The instanton-induced cross section turns out to be in a measurable range [9, 10, 14], $\sigma_{\text{HERA}}^{(I)} \approx \mathcal{O}(30 \div 100)$ pb, depending on cuts. Crucial information on the region of validity for this important result, based on instanton-perturbation theory, comes from a recent high-quality lattice simulation [10]. The main event signatures comprise a “fireball”-like final state with a very high number of hadrons, including K mesons and Λ hyperons, as well as a high total transverse energy². With the help of the Monte Carlo generator QCDINS for QCD-instanton-induced events in deep-inelastic scattering [12], the H1 and ZEUS experiments at HERA are actively searching for signatures of instantons in the hadronic final state. The challenging experimental task is to distinguish the instanton-induced signal from the normal DIS final state near the edge of the available phase space. This effort seems however well worthwhile, since an experimental verification of such a novel, non-perturbative manifestation of QCD would be of basic significance.

At the recent DIS2000 and ICHEP2000 conferences, the H1 collaboration has reported preliminary results of a first dedicated search for instanton-induced events at HERA [15, 16]. In a phase space region, where a reduction of the normal DIS (nDIS) background to the percent level is achieved according to standard Monte Carlo models, a (statistically) significant excess of events was found in the H1 data. While its size is at a level still comparable to the differences among standard DIS event generators, it is - for the discriminating observables - qualitatively similar to the expected instanton signal. The results presented are quite intriguing and encouraging, although far from being conclusive. Yet, they strongly enhance the motivation for looking more closely at some remaining theoretical issues related to our original predictions.

2. Let us start off by briefly summarizing the strategy and essential results of the H1 search for instanton-induced events [15, 16]. Structure and kinematical variables of the dominant instanton-induced process in deep-inelastic scattering are displayed in Fig. 1. Of particular importance will be the Bjorken-variables (Q'^2, x') of the so-called instanton subprocess $q' + g \Rightarrow I \Rightarrow X$.

The H1 analysis is based on the strategy [11] of isolating an “instanton-enriched” data sample by

¹For an exploratory calculation of the instanton contribution to the gluon-structure function, see Ref. [13].

²A more extensive introduction to instanton-induced events in DIS may e.g. be found in Ref. [14].

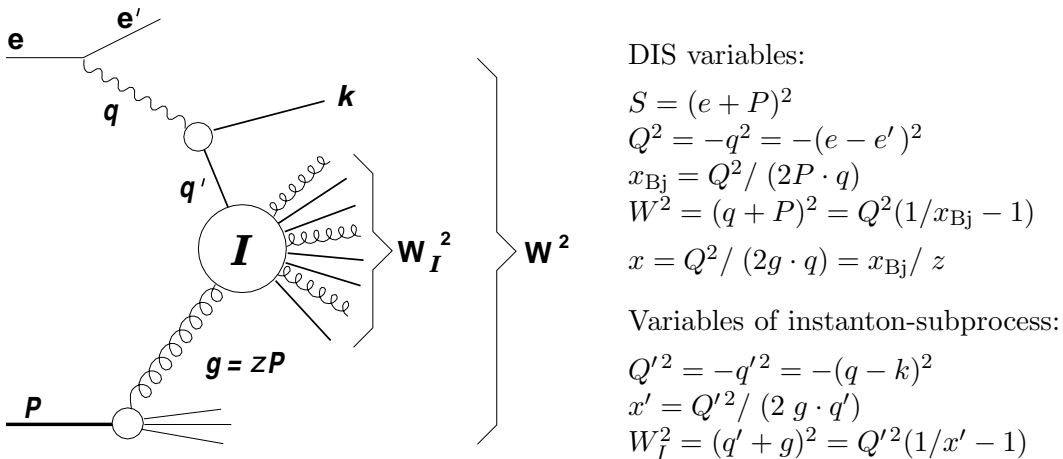


Figure 1: Structure and kinematic variables of the dominant instanton-induced process in deep-inelastic scattering.

means of suitable cuts to a set of three sensitive, discriminating observables, defined in Table 1 (left). Three different cut-scenarios A), B) and C) with *increasing* instanton-separation power $\epsilon_I/\epsilon_{\text{nDIS}}$ were defined according to

- A) the highest instanton efficiency (ϵ_I);
- B) high ϵ_I at reasonable normal DIS background reduction (normal DIS efficiency ϵ_{nDIS});
- C) highest instanton-separation power at $\epsilon_I \approx 10\%$.

In all three cut-scenarios, significantly more events are observed than expected by standard DIS Monte Carlo models. It is noteworthy that with increasing instanton-separation power an increasingly large excess is seen in the data. The H1 collaboration has compared the observed excess

Observables		
$n_{\text{ch,b}}$ = number of charged particles in “instanton band”	Et_{b} =	total transverse energy in “instanton band”
Sph = sphericity in the rest system of particles not from current jet	$1 - E_{\text{out,b}}/E_{\text{in,b}}$ =	Et -weighted azimuthal event isotropy
$Q_{\text{rec}}'^2$ = reconstructed virtuality of quark entering I -subprocess	Et_{jet} =	transverse energy of current jet

Table 1: Set of discriminating instanton-sensitive observables as used by the H1 collaboration [15, 16]. Instanton-enhancement cuts are applied to the three observables on the left. All observables refer to the hadronic CMS ($\vec{q} + \vec{P} = \vec{0}$), except for the sphericity that is calculated in the rest system of the particles not belonging to the current jet. The latter is identified with the jet of highest Et . The “instanton band” is a prominent theoretical prediction [7, 14] and is experimentally placed at $\bar{\eta} \pm 1.1$ where $\bar{\eta}$ is the Et -weighted mean pseudorapidity of all particles not belonging to the current jet.

in each of the six observables (Table 1) to our predictions from the QCDINS 2.0 Monte Carlo generator [12]. It is found that the shape and the size of the excess in the three discriminating observables $n_{\text{ch},b}$, Sph and $Q'_{\text{rec}}{}^2$ with instanton-enhancement cuts, as well as in the azimuthal event isotropy $1 - E_{\text{out},b}/E_{\text{in},b}$, are in qualitative agreement with the expected instanton signal. However, the comparison with the two remaining observables, Et_b and Et_{jet} , is more involved. While there appears to be also a marked excess in the respective data, both $\langle Et_b \rangle$ and $\langle Et_{\text{jet}} \rangle$ appear to be shifted towards smaller values than predicted by QCDINS, and the widths of the experimental distributions are also considerably narrower.

Figure 2 may serve as an illustration of the achievable instanton signature in the set of six instanton-sensitive observables (c. f. Table 1) with cuts, integrated luminosity ($\int \mathcal{L} dt = 15.8 \text{ pb}^{-1}$) and parton densities [17] as for the preliminary H1 data [15, 16]. While refraining to show the real data before their final publication, we have instead displayed the statistical errors as calculated by means of the HERWIG 5.9 [18] event generator for vanishing excess. On the one hand, the corresponding number of 361 ± 26 nDIS events from HERWIG after instanton-enhancement cuts (cut-scenario **C** [15, 16]) matches quite well the values quoted by the H1 collaboration. On the other hand, the detector corrections (not accounted for here) seem to significantly reduce the number of instanton events by almost a factor of two.

A central issue to be discussed in this letter is the question to which extent the H1 analysis may be directly compared to our theoretical predictions, since certain fiducial cuts are lacking in the H1 data: Because of difficulties with the x' -reconstruction, there is presently no cut on x' , while the data are compared to QCDINS with the default x' -cut implemented. Moreover, both the data and the QCDINS results used are lacking the theoretically required cut in $Q^2 \gtrsim \mathcal{O}(100) \text{ GeV}^2$. We also use this opportunity to reconsider in some detail the theoretical uncertainties due to the extraction of the fiducial cuts in (Q'^2, x') from lattice data and due to the known uncertainties $\delta\Lambda_{\overline{\text{MS}}}$ of the QCD scale.

3. Proceeding in reverse order for reasons of presentation, let us turn first to the uncertainties arising from $\delta\Lambda_{\overline{\text{MS}}}$ via the known strong dependence [9] of the instanton subprocess cross section (c. f. Fig. 1) on the QCD scale parameter,

$$\sigma_{q'g}^{(I)}(Q'^2, x') \propto \left(\frac{\Lambda_{\overline{\text{MS}}}^2}{Q'^2} \right)^{\beta_0 F(x')} ; \quad \beta_0 = 11 - \frac{2}{3}n_f; \quad 1/2 \leq F(x') \leq 1. \quad (1)$$

The dependence of the various observables on the uncertainty of $\Lambda_{\overline{\text{MS}}}^{(n_f=3)}$ is displayed in Fig. 2. The solid line corresponds to the default prediction of our QCDINS event generator [12], with $\Lambda_{\overline{\text{MS}}}^{(3)} = 346_{-29}^{+31} \text{ MeV}$, being obtained by “flavour reduction” with 3-loop accuracy from the 1998 world-average value [19] $\Lambda_{\overline{\text{MS}}}^{(5)} = 219_{-23}^{+25} \text{ MeV}$ or $\alpha_s(M_Z) = 0.119 \pm 0.002$. Note that the errors quoted for the total expected instanton-event numbers in Fig. 2 only refer to these $\Lambda_{\overline{\text{MS}}}^{(5)}$ uncertainties. The optimization of the instanton-enhancement cuts (cut-scenario **C** of Ref. [15, 16]) reflects in the number of instanton events being maximal for the default value of $\Lambda_{\overline{\text{MS}}}^{(5)}$.

Apparently, the actual dependence of the various observables on $\delta\Lambda_{\overline{\text{MS}}}^{(3)}$ is much less dramatic than naively expected from Eq. (1). The reason is, of course, associated with the fact that the fiducial

Cuts		Instanton Events ($\int \mathcal{L} dt = 15.8 \text{ pb}^{-1}$)	$\Lambda_{\overline{\text{MS}}}^{(n_f=3)}$ [MeV]
fiducial (theory):	$x' \geq 0.35, Q'/\Lambda_{\overline{\text{MS}}}^{(n_f)} \geq 30.8$	633 $^{-154}_{+194}$	346 $^{+31}_{-29}$
kinematical:	$x_{\text{Bj}} \geq 10^{-3}, 0.1 \leq y_{\text{Bj}} \leq 0.6,$ $\theta_{el} > 156^\circ, E'_{el} \geq 10 \text{ GeV}$		
instanton enhancement: (cut-scenario C [15, 16])	$n_{\text{ch,b}} \geq 8, \text{Sph} > 0.5,$ $105 < Q'^2_{\text{rec}} < 200 \text{ GeV}^2$	163 $^{-23}_{-28}$	

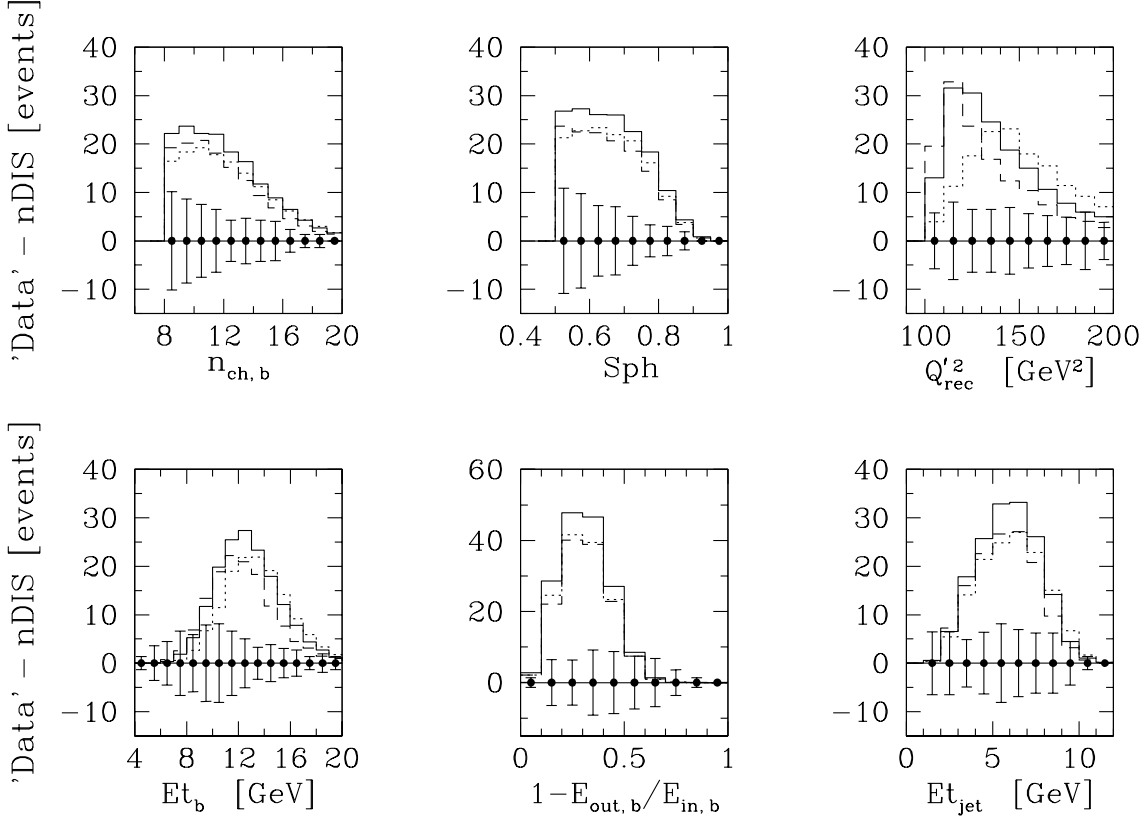


Figure 2: Predicted excess due to instanton-induced events (QCDINS 2.0 [12]), relative to the normal DIS expectations (nDIS). Except for missing detector corrections, all cuts, luminosity (c. f. Table above), observables (c. f. Table 1) and the parton densities [17] are as for the preliminary H1 data [15, 16]. While refraining to show the real data before their final publication, we have instead displayed the statistical errors as calculated by means of the HERWIG 5.9 [18] event generator for vanishing excess. Apart from modelling the achievable significance of the instanton signal via a good approximation of the actual (statistical) errors, the figure displays the dependence of the various observables on the uncertainty of $\Lambda_{\overline{\text{MS}}}^{(3)}$. The solid, dotted and dashed lines refer to the 1998 world average value $\Lambda_{\overline{\text{MS}}}^{(5)} = 219 \text{ MeV}$ [19], its upper and lower 1σ limits, respectively.

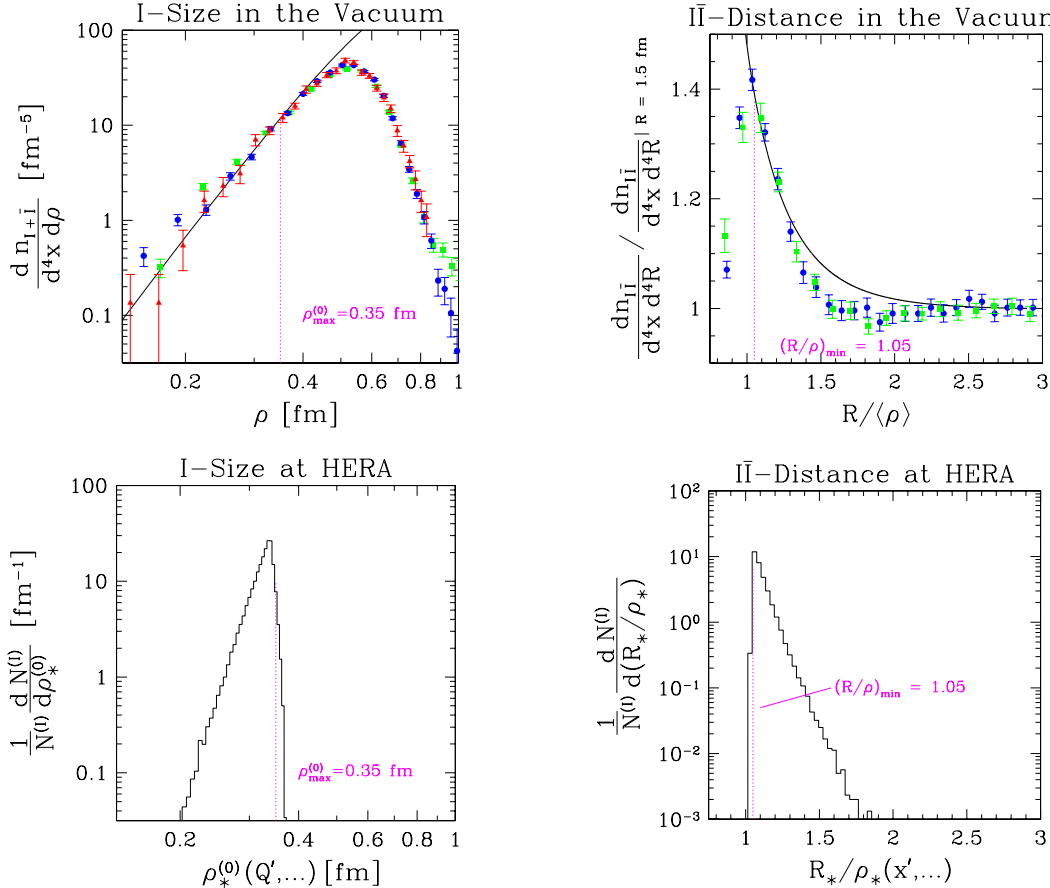


Figure 3: Top: Illustration of the agreement of recent high-quality lattice data [3, 10] for the instanton-size distribution and the $\bar{I}\bar{I}$ -distance distribution with the predictions from instanton-perturbation theory [10] for $\rho \lesssim 0.35$ fm and $R/\rho \gtrsim 1.05$, respectively. Bottom: Display of the instanton-induced event distributions for HERA from QCDINS, as function of the saddle-point values $(\rho_*(Q', \dots), R_*/\rho_*(x', \dots))$, with the default (Q'^2, x') -cuts implemented as in Fig. 2. In these variables, the above cut-off values $(\rho_{\max}^{(0)}, (R/\rho)_{\min})$ extracted from the lattice are apparent.

Q' -cut in Fig. 2 is proportional to $\Lambda_{\overline{\text{MS}}}^{(3)}$. This is a natural consequence from exploiting lattice results to which we shall turn next.

4. Let us reconsider [9, 10] in more detail the extraction of the fiducial cuts in (Q', x') from a recent high-quality lattice simulation of quenched QCD [3], with special emphasis on the major associated uncertainties³.

The validity of instanton-perturbation theory, on which our predictions for HERA are based, requires instantons of small enough size $\rho \leq \rho_{\max}$ along with a sufficiently large separation $R/\rho \geq (R/\rho)_{\min}$ between them. Crucial information on $(\rho_{\max}, (R/\rho)_{\min})$ was obtained [10] by confronting the predictions of instanton-perturbation theory with the UKQCD lattice “data” [3] for the I -size distribution $\frac{dn_I}{d^4x d\rho}$ and the $\bar{I}\bar{I}$ -distance distribution $\frac{dn_{\bar{I}\bar{I}}}{d^4x d^4R}$ (c.f. Fig. 3 (top)).

³ A proper account of the considerable systematic uncertainties associated with different cooling/smoothing methods in the lattice simulations [3, 5] and [4] is very hard and clearly beyond the scope of this paper.

Let us recall [9, 10] that the instanton-induced cross section $\sigma_{\text{HERA}}^{(I)}$ depends strongly on these lattice observables via Fourier-type transformations⁴,

$$\sigma_{q'g}^{(I)}(Q'^2, x') \sim \int d^4R e^{i(p+q') \cdot R} \underbrace{\int_0^\infty d\rho \int_0^\infty d\bar{\rho} \underbrace{D(\rho) D(\bar{\rho})}_{\frac{dn_I}{d^4x d\rho}} \int dU e^{-\frac{4\pi}{\alpha_s} \Omega\left(\frac{R^2}{\rho\bar{\rho}}, \frac{\bar{z}}{\rho}, U\right)} e^{-Q'(\rho+\bar{\rho})}}_{\frac{dn_{I\bar{I}}}{d^4x d^4R}} \{\dots\}. \quad (2)$$

Due to this structure, the limits $(\rho_{\max}, (R/\rho)_{\min})$ for the validity of instanton-perturbation theory from lattice data may, in fact, be translated in a one-to-one manner, via a saddle-point relation, to *minimally required cuts* on the conjugate Bjorken variables (Q'^2, x') of the instanton-subprocess as follows,

$$\left. \begin{array}{l} \frac{Q'_{\min}}{\Lambda_{\overline{\text{MS}}}^{(n_f)}} \\ x'_{\min} \end{array} \right\} \text{saddle-point} \Leftrightarrow \left\{ \begin{array}{l} \frac{\beta_0^{(n_f)}}{\Lambda_{\overline{\text{MS}}}^{(n_f)}} \frac{1}{\rho_{* \max}^{(n_f)}} \approx \frac{\beta_0^{(0)}}{\Lambda_{\overline{\text{MS}}}^{(0)}} \frac{1}{\rho_{\max}^{(0)}}; \\ \left(\frac{R_*}{\rho_*}\right)_{\min}^{(n_f)} \approx \left(\frac{R}{\rho}\right)_{\min}^{(0)}. \end{array} \right. \quad (3)$$

According to the known n_f -dependence of the solutions (ρ_*, R_*) of the saddle-point equations [9], one finds that the combinations $(\rho_* \Lambda_{\overline{\text{MS}}}/\beta_0, R_*/\rho_*)$ are approximately n_f -independent functions of $(Q'/\Lambda_{\overline{\text{MS}}}, x')$. In addition, Eq. (3) incorporates the working hypothesis that the n_f -independence of this combination extends also to the corresponding limits of validity of instanton-perturbation theory. With high-quality lattice data being only available for $n_f = 0$ at present, this appears to be a near-at-hand prescription to account for effects of light flavours in the required fiducial cuts. In practice, one will identify the actual (Q', x') cuts with the “fiducial” ones, i.e. (Q'_{\min}, x'_{\min}) , in order to profit from a high event rate without losing theoretical control.

Before turning to a discussion of uncertainties associated with this procedure, let us briefly recapitulate the main result on the fiducial region from Ref. [10] and its implementation in the QCDINS [12] event generator for HERA. First of all, Fig. 3 (top) illustrates the good agreement of the data for the instanton-size distribution and the $I\bar{I}$ -distance distribution from Refs. [3, 10] with the predictions from instanton-perturbation theory from Refs. [10, 12], for

$$\left. \begin{array}{l} \rho \lesssim \rho_{\max}^{(0)} \approx 0.35 \text{ fm}; \\ \frac{R}{\rho} \gtrsim \left(\frac{R}{\rho}\right)_{\min} \approx 1.05; \end{array} \right\} \text{implying} \left\{ \begin{array}{l} Q'/\Lambda_{\overline{\text{MS}}}^{(n_f)} \gtrsim 30.8; \\ x' \gtrsim 0.35. \end{array} \right. \quad (4)$$

Figure 3 (bottom) displays the instanton-induced event distribution for HERA from QCDINS, as function of the saddle-point values $(\rho_*^{(0)}(Q', \dots), R_*/\rho_*(x', \dots))$, with default fiducial cuts in (Q'^2, x') as in Fig. 2 (top). Apparently, the event distribution correctly reflects the above cut-off values $(\rho_{\max}^{(0)}, (R/\rho)_{\min})$ extracted from the lattice.

The next issue is to extract a more quantitative estimate for the associated uncertainties. Starting with the ρ -dependence in the I -size distribution, we also take into account the error on the QCD-scale parameter $\Lambda_{\overline{\text{MS}}}^{(0)}$ for $n_f = 0$ from Ref. [20] as follows. We treat $\Lambda_{\overline{\text{MS}}}^{(0)}$ as a free parameter

⁴In Eq. (2), D , Ω and $\{\dots\}$ denote the known theoretical expressions for the I -size distribution, the $I\bar{I}$ -valley interaction and further smooth factors, respectively.

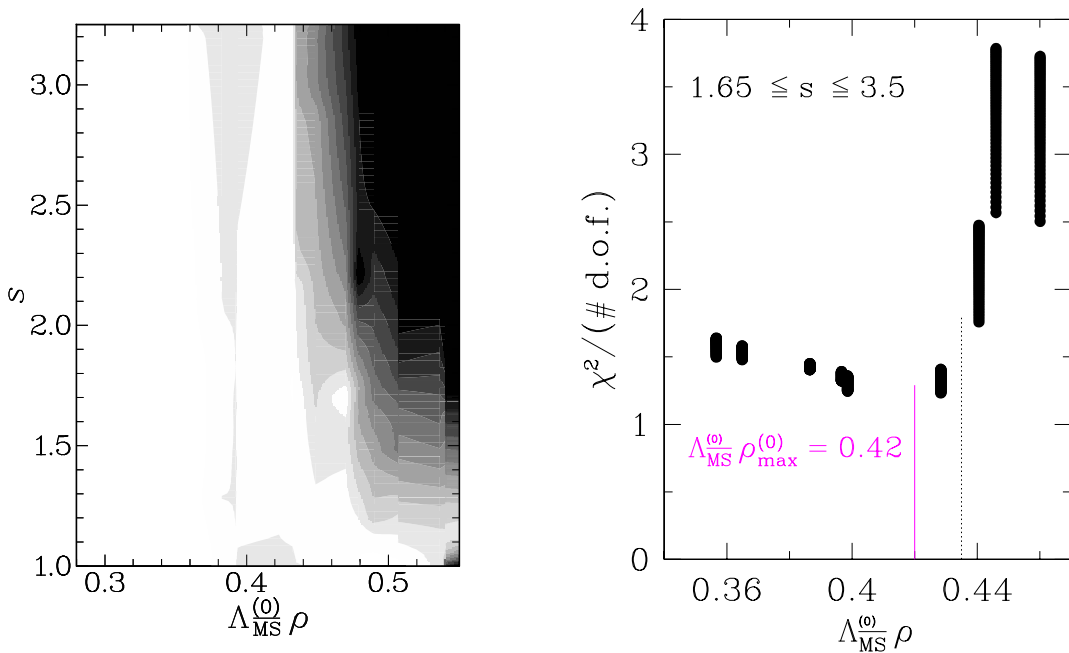


Figure 4: $\chi^2/(\# \text{ d.o.f.})$, characterizing the deviation of instanton-perturbation theory from the UKQCD lattice data [3, 10] for the I -size distribution according to Eq. (5). Left: Contour plot for a range of maximal values of $\Lambda_{\overline{\text{MS}}}^{(0)}\rho$ and of the renormalization-scale factor s . Darker shading corresponds to increasing $\chi^2/(\# \text{ d.o.f.})$. Right: Projection on the $\Lambda_{\overline{\text{MS}}}^{(0)}\rho$ -axis for a range of larger s -values. The solid line corresponds to the default $\Lambda_{\overline{\text{MS}}}^{(0)}\rho$ cut-off in QCDINS 2.0 and the dotted one to an estimate of the associated uncertainty.

fluctuating around its quoted mean value, $\langle \Lambda_{\overline{\text{MS}}}^{(0)} \rangle = 238 \text{ MeV}$, with error $\delta \Lambda_{\overline{\text{MS}}}^{(0)} = 19 \text{ MeV}$, in the following χ^2 function,

$$\chi^2(\Lambda_{\overline{\text{MS}}}^{(0)}\rho, s) = \min_{\Lambda_{\overline{\text{MS}}}^{(0)}} \left\{ \sum_{\rho_i \leq \rho} \left(\frac{\frac{dn_{I+\bar{I}}(\rho_i)}{d^4x d\rho} - 2 D_{I-\text{pert.th.}}(\rho_i, s, \Lambda_{\overline{\text{MS}}}^{(0)})}{\delta \frac{dn_{I+\bar{I}}(\rho_i)}{d^4x d\rho}} \right)^2 + \left(\frac{\Lambda_{\overline{\text{MS}}}^{(0)} - \langle \Lambda_{\overline{\text{MS}}}^{(0)} \rangle}{\delta \Lambda_{\overline{\text{MS}}}^{(0)}} \right)^2 \right\}. \quad (5)$$

The theoretical expression for the I -size distribution $D_{I-\text{pert.th.}}(\rho_i, s, \Lambda_{\overline{\text{MS}}}^{(0)})$ from instanton-perturbation theory is taken as in Ref. [10]. It incorporates renormalization-group invariance at the two-loop level, $d \ln(D(\rho, s, \Lambda_{\overline{\text{MS}}}^{(0)}))/d \ln(s) = \mathcal{O}(\alpha_s^2)$, with the renormalization-scale dependence parametrized conveniently as

$$\mu = s/\rho. \quad (6)$$

The resulting $\chi^2/(\# \text{ d.o.f.})$, minimized with respect to $\Lambda_{\overline{\text{MS}}}^{(0)}$, is displayed in Fig. 4 for a range of maximal values of $\Lambda_{\overline{\text{MS}}}^{(0)}\rho$ and of the renormalization-scale factor s . First of all, it is important to consider sufficiently large $s > 1$, where the incorporated two-loop renormalization-group invariance should lead to a largely s -independent limit $\rho_{\text{max}}^{(0)}$. Indeed, this is nicely reflected in the contour-plot of the resulting $\chi^2/(\# \text{ d.o.f.})$ versus s and $\Lambda_{\overline{\text{MS}}}^{(0)}\rho$ in Fig. 4 (left). The projection on the $\Lambda_{\overline{\text{MS}}}^{(0)}\rho$ -axis for $1.65 \leq s \leq 3.5$ in Fig. 4 (right) indicates a fairly sharp increase of $\chi^2/(\# \text{ d.o.f.})$

around $\Lambda_{\overline{\text{MS}}}^{(0)}\rho \approx 0.42$, corresponding to our previous default cut-off $\rho_{\text{max}}^{(0)} \approx 0.35$ fm. As a semi-quantitative upper limit for $\rho_{\text{max}}^{(0)}$ one may use the value, where the probability corresponding to $\chi^2/(\#\text{ d.o.f.})$ has dropped from⁵ $\mathcal{O}(20)\%$ to 5%. In this way, we find

$$\Lambda_{\overline{\text{MS}}}^{(0)}\rho_{\text{max}}^{(0)} = 0.42 \div 0.435, \quad \text{implying} \quad \frac{Q'_{\text{min}}}{\Lambda_{\overline{\text{MS}}}^{(n_f)}} = 28.2 \div 30.8. \quad (7)$$

As to the R/ρ -dependence of the $I\bar{I}$ -distance distribution in Fig. 3 (top, right), a naked-eye estimate for the uncertainty in $(R/\rho)_{\text{min}}$ gives the range

$$\left(\frac{R}{\rho}\right)_{\text{min}} = 1.0 \div 1.05, \quad \text{implying} \quad x'_{\text{min}} = 0.31 \div 0.35. \quad (8)$$

More quantitative methods do not seem worthwhile here, due to remaining theoretical ambiguities [10]: The integrations over the I - and \bar{I} -sizes in the $I\bar{I}$ -distance distribution (c.f. Eq. (2)) imply significant contributions also from larger instantons with $0.35 \text{ fm} \lesssim \rho, \bar{\rho} \lesssim 0.6 \text{ fm}$, say.

5. Let us now turn to the crucial question to which extent the H1 analysis may be directly compared to our theoretical predictions. As mentioned earlier, possibly important fiducial cuts are lacking in the H1 data. Firstly, we address the fact that there is presently no cut on x' in the data, while these are compared to our QCDINS predictions with the default x' -cut implemented.

A glance at the lattice data for the $I\bar{I}$ -distance distribution (Fig. 3 (top, right)) reveals that actually, instanton-effects seem to be very strongly suppressed, as soon as instantons and anti-instantons start “touching” each other, i.e. for small enough separation, $R/\rho \leq \mathcal{O}(1)$. This rapid onset of instanton suppression corresponds to $x' \lesssim 0.35$, which happens to coincide with our default x' -cut. Hence, since our QCDINS predictions, *with* the x' -cut implemented, model quite well the actual suppression (c.f. Fig. 3 (top, right) and (bottom, right)), we consider the lacking experimental reconstruction of x' not a serious problem in principle.

Quantitatively speaking, however, the lacking experimental x' -cut leads to a quite substantial ambiguity in the expected *size* of the instanton signal in the various observables. In this case, the onset of the actual instanton suppression from Fig. 3 (top, right), modelled by an x' -cut within the allowed theoretical x'_{min} -uncertainty window (8), gives rise to a possible increase of the size of the instanton signal up to a factor of three compared to our default prediction. This is displayed in Fig. 5 (left). Yet, the predicted *shapes* of the six distributions in Fig. 2 are virtually unaffected by this important remaining uncertainty. Upon variation of x'_{min} within the window (8), we note that to very good approximation, the predicted instanton-induced excess in all six H1 observables of Fig. 2 varies by the *common* factor displayed in Fig. 5 (left) for cut-scenario **C**. In particular, a slight reduction, $x'_{\text{min}} = 0.325$, compared to the QCDINS default x' -cut, leads to an increase of the instanton signal by a factor of two, representing a remarkably good description of the observed excess in four ($n_{\text{ch,b}}$, Sph, $Q'_{\text{rec}}{}^2$ and $1 - E_{\text{out,b}}/E_{\text{in,b}}$) out of the six experimentally considered observables. While the size of the observed excess in the remaining two observables Et_{b} and Et_{jet} is quite satisfactorily described as well, both $\langle Et_{\text{b}} \rangle$ and $\langle Et_{\text{jet}} \rangle$ appear to be shifted towards smaller values than predicted by QCDINS, and the widths of the experimental distributions are

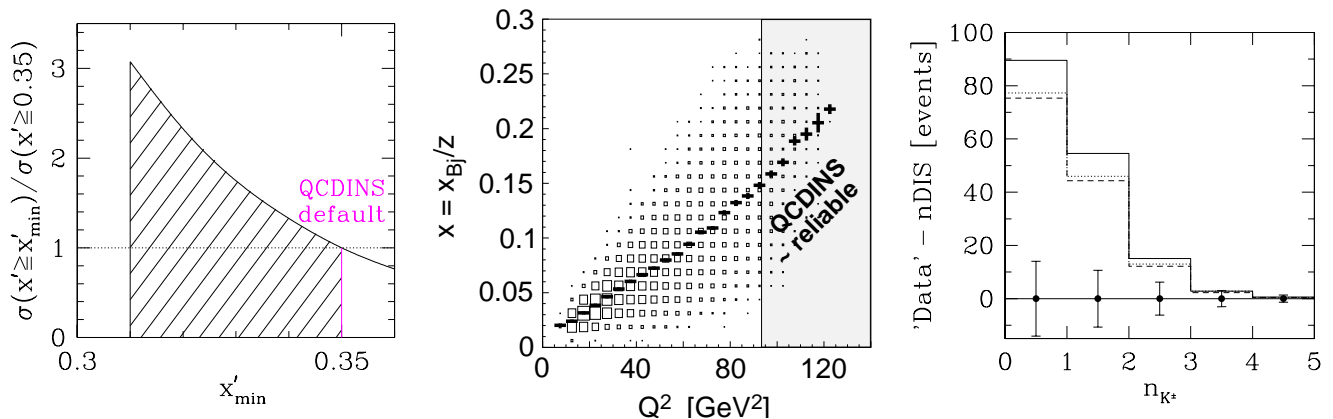


Figure 5: Left: Common enhancement factor for the instanton signal in all six H1 observables (Table 1, Fig. 2, cut-scenario **C**), arising upon variation of the x' -cut within the allowed uncertainty window (8). Middle: Illustration of the strong $x - Q^2$ -correlation according to QCDINS for cut-scenario **C**. The strong concentration of events around $(x \approx 0.035, Q^2 \approx 20 \text{ GeV}^2)$ is apparent. Right: Predicted excess of charged kaons due to instanton-induced events according to QCDINS [12], relative to the normal DIS expectations (nDIS). The meaning of the various lines, the statistical errors, cuts and luminosity are as in Fig. 2.

also considerably narrower.

We shall argue next that this apparent discrepancy is actually a consequence of the experimentally lacking but theoretically required cut in Q^2 ,

$$Q^2 \geq Q_{\min}^2 \approx Q_{\min}'^2 = \mathcal{O}(100) \text{ GeV}^2. \quad (9)$$

As a brief reminder [8, 12], this cut assures in particular the dominance of “planar” handbag-type graphs in $\sigma_{\text{HERA}}^{(I)}$ and all final-state observables. The non-planar contributions do not share the simple, probabilistic interpretation of the planar ones, involve instantons with a size determined by $1/Q$ rather than $1/Q'$ and are both hard to calculate and hard to implement in a Monte Carlo generator. On account of their known power suppression in $1/Q^2$ and a cross-check in the simplest case without final-state gluons [8], they can be safely neglected upon application of the cut (9). Because of these reasons, the non-planar contributions are not implemented in QCDINS.

In order to gain some further insight as to the influence of this Q^2 -cut, consider Et_{jet} , for example, for which one may easily derive the following simple expression on the parton level in the hadronic CMS,

$$Et_{\text{jet}} = Q' \sqrt{1 - \frac{x}{x'}} \sqrt{1 - \frac{x}{x'} \frac{Q'^2}{Q^2}}, \quad (10)$$

involving besides Q^2 , Q'^2 and x' , the Bjorken- x of the $\gamma^* g \Rightarrow X$ subprocess in Fig. 1. The important issue to be exploited next is the strong correlation between Q^2 and x , apparent in Fig. 5 (middle). Already at this point, it is clear that via its x -dependence (10), the Et_{jet} -distribution is strongly dependent on the underlying Q^2 -spectrum. In absence of the theoretically

⁵Clearly, the absolute value of the probability is not very meaningful, since, for the three lattice data sets used, the unknown but significant systematical errors have been ignored.

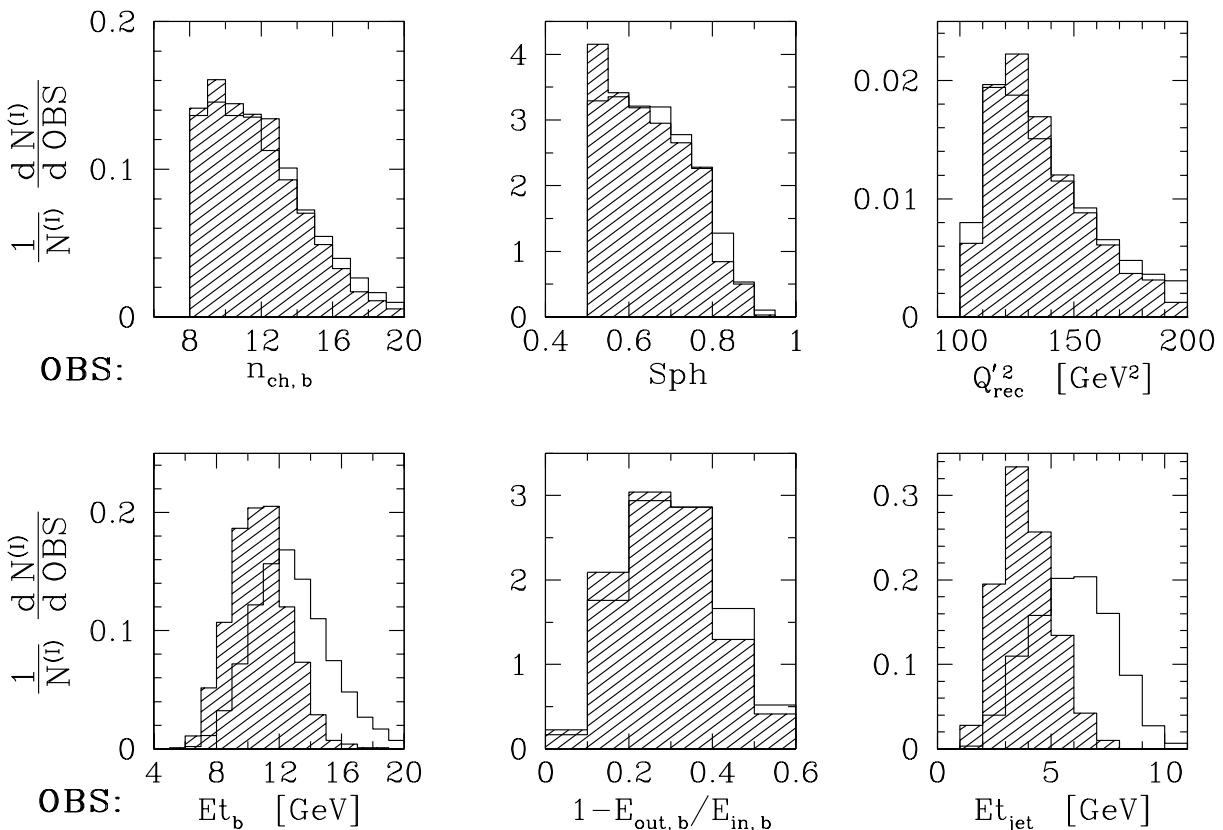


Figure 6: Dependence of the shape-normalized distributions of the six H1 observables (Table 1, Fig. 2) for cut-scenario **C** on the low- Q^2 portion of the spectrum, for which QCDINS is not reliable. The shaded distributions are obtained with an additional cut $x \geq 0.15$, depleting the low- Q^2 regime. Note the resulting substantial shift and narrowing of the Et_{jet} and Et_b distributions, with the remaining ones being largely unaffected.

required cut in Q^2 , the x -distribution peaks sharply around $\langle x \rangle \approx 0.035$ according to QCDINS and involves a fairly small $\langle Q^2 \rangle \approx 20 \div 30 \text{ GeV}^2$ (c.f. Fig. 5 (middle)). In fact, this dominating and theoretically uncontrollable low- Q^2 portion of the spectrum is responsible for the Et_{jet} -peak being located at too large a value, since

$$\text{with } \left\{ \begin{array}{l} \langle x' \rangle \approx x'_{\min} = 0.35 \\ \langle Q'^2 \rangle \approx Q'^2_{\min} \approx 113 \text{ GeV}^2 \end{array} \right\} \xrightarrow{\text{Eq. (10)}} \langle Et_{\text{jet}} \rangle = \mathcal{O}(6) \text{ GeV}, \quad (11)$$

in good agreement with the direct (but unreliable) result from QCDINS in Fig. 2, not involving a cut in Q^2 .

With this insight, let us perform the following exercise. We deplete the low- Q^2 portion of the spectrum by means of a cut, $x \geq 0.15$, in the (internal) Bjorken- x variable. The QCDINS results should now be about reliable since from Fig. 5 (middle) we have effected a shift to $\langle Q^2 \rangle \approx 95 \text{ GeV}^2$. The striking result of this exercise is shown in Fig. 6 for the six shape-normalized distributions of the H1 observables. First of all, we observe that the shapes of the four distributions of $n_{\text{ch,b}}$, Sph , Q'^2_{rec} and $1 - E_{\text{out,b}}/E_{\text{in,b}}$, for which there was good agreement with the observed excess before applying the x -cut, remain essentially unaffected. Their shapes are thus rather insensitive

to the Q^2 -spectrum and should be reliably predicted by QCDINS, even without application of the required cut in Q^2 . On the contrary, the shape-normalized distributions of Et_{jet} and Et_b appear both shifted significantly towards smaller values and are now much narrower. Notably, the shape-normalized Et_{jet} -distribution is now in virtually perfect agreement with the corresponding experimental quantity. Also the Et_b -distribution matches well the experimental trend, after this depletion of the low- Q^2 region.

On the one hand, these arguments may well serve as indication that upon proper implementation of the required fiducial cuts the good description of the data will persist. On the other hand, they should be taken as a strong encouragement to try and implement the lacking cuts in Q^2 and x' into the data. The essential, remaining problematic is that searches for an instanton-induced excess in DIS have to rely on background estimates from nDIS Monte Carlo generators, in a region of phase space where their accuracy is not too well known.

We close with a reminder of our predictions for the rate of charged kaons that can and should be investigated by means of dE/dx in the instanton-enhanced data sample (c.f. Fig. 5 (right) for cut-scenario **C**). An excess of kaons, as direct consequence of the flavour democracy of the instanton-induced interaction, represents a crucial independent signature. Respective data will hopefully be included in the final H1 analysis.

Acknowledgements

We wish to thank our experimental colleagues Volker Blobel for advice on statistical methods, Tancredi Carli for many helpful discussions and active collaboration and Eckhard Elsen for a careful reading of the manuscript.

References

- [1] A. Belavin *et al.*, Phys. Lett. B 59 (1975) 85.
- [2] G. 't Hooft, Phys. Rev. D 14 (1976) 3432.
- [3] D.A. Smith and M.J. Teper (UKQCD Collab.), Phys. Rev. D 58 (1998) 014505.
- [4] A. Hasenfratz and C. Nieter, Phys. Lett. B 439 (1998) 366.
- [5] P. de Forcrand, M. Garcia Perez, J. Hetrick and I. Stamatescu, Nucl. Phys. Proc. Suppl. 63 (1998) 549.
- [6] T. Schäfer and E. Shuryak, Rev. Mod. Phys. 70 (1998) 323 and references cited therein.
- [7] A. Ringwald and F. Schrempp, hep-ph/9411217, in *Quarks '94*, eds. D. Yu. Grigoriev *et al.* (World Scientific, Singapore, 1995).
- [8] S. Moch, A. Ringwald and F. Schrempp, Nucl. Phys. B 507 (1997) 134.

- [9] A. Ringwald and F. Schrempp, Phys. Lett. B 438 (1998) 217.
- [10] A. Ringwald and F. Schrempp, Phys. Lett. B 459 (1999) 249.
- [11] T. Carli, J. Gerigk, A. Ringwald and F. Schrempp, hep-ph/9906441, in *Monte Carlo Generators for HERA Physics*, eds. A.T. Doyle *et al.*, DESY-PROC-1999-02.
- [12] A. Ringwald and F. Schrempp, Comput. Phys. Commun. 132 (2000) 267.
- [13] I. Balitsky and V. Braun, Phys. Lett. B 314 (1993) 237
- [14] A. Ringwald and F. Schrempp, hep-ph/9909338, in *New Trends in HERA Physics 1999*, eds. G. Grindhammer *et al.* (Springer, 2000).
- [15] S. Mikocki (for the H1 Collaboration), hep-ex/0007008, to appear in *Proc. 8th Int. Workshop on Deep Inelastic Scattering and QCD (DIS 2000)*, Liverpool, England, April 25-30, 2000.
- [16] H1 collaboration, contr. paper to 30th Int. Conf. on High Energy Physics (ICHEP 2000), Osaka, Japan, July 27 - August 2, 2000,
<http://www-h1.desy.de/psfiles/confpap/ICHEP2000/H1prelim-00-025.ps>.
- [17] H.L. Lai *et al.* (CTEQ Collab.), Phys. Rev. D 55 (1997) 1280.
- [18] G. Marchesini *et al.*, Comput. Phys. Commun. 67 (1992) 465.
- [19] C. Caso *et al.* (Particle Data Group), Eur. Phys. J. C 3 (1998) 1.
- [20] S. Capitani, M. Lüscher, R. Sommer and H. Wittig, Nucl. Phys. B 544 (1999) 669.